

# A Versatile Toolkit for Controllable and Highly Selective Multifunctionalization of Bacterial Magnetic Nanoparticles

Frank Mickoleit, Clarissa Lanzloth, and Dirk Schüler\*

Their unique material characteristics, i.e. high crystallinity, strong magnetization, uniform shape and size, and the ability to engineer the enveloping membrane *in vivo* make bacterial magnetosomes highly interesting for many biomedical and biotechnological applications. In this study, a versatile toolkit is developed for the multifunctionalization of magnetic nanoparticles in the magnetotactic bacterium *Magnetospirillum gryphiswaldense*, and the use of several abundant magnetosome membrane proteins as anchors for functional moieties is explored. High-level magnetosome display of cargo proteins enables the generation of engineered nanoparticles with several genetically encoded functionalities, including a core-shell structure, magnetization, two different catalytic activities, fluorescence and the presence of a versatile connector that allows the incorporation into a hydrogel-based matrix by specific coupling reactions. The resulting reusable magnetic composite demonstrates the high potential of synthetic biology for the production of multifunctional nanomaterials, turning the magnetosome surface into a platform for specific versatile display of functional moieties.

## 1. Introduction

Bacterial magnetosomes are specialized intracellular organelles, which are synthesized by magnetotactic bacteria for orientation along geomagnetic field lines. In the alphaproteobacterium *Magnetospirillum gryphiswaldense* and related bacteria they consist of an inorganic, monocrystalline core of magnetite (Fe<sub>3</sub>O<sub>4</sub>), enveloped by a biological membrane that contains phospholipids and a set of magnetosome specific proteins. The latter fulfill various functions in and exert strict biological control over magnetosome biosynthesis.<sup>[1–5]</sup> In addition, biomineralized crystals exhibit characteristics superior compared to those of abiogenic (i.e., inorganic, chemically synthesized) nanoparticles. Under optimal, low-oxygen conditions, magnetotactic bacteria synthesize magnetosomes that possess a narrow size distribution and uniform morphology. Usually, the particles are large single magnetic domain nanoparticles with a strong magnetization and a stable

magnetic moment at physiological temperatures. The magnetite core itself is of high purity and crystallinity, being protected against oxidation processes by the surrounding magnetosome membrane.<sup>[6–11]</sup> These features and their natural biocompatibility make magnetosomes a promising tool for numerous biotechnological and biomedical applications, such as nanocarriers in magnetic drug targeting, magnetosome-based immunoassays, as reporters for magnetic resonance imaging (MRI) or for magnetic hyperthermia.<sup>[3,12–14]</sup>

Many of these applications require further functionalities, resulting in a strong need for a tunable, specific magnetosome display system that allows the simultaneous and selective addition of several functional moieties to the particle surface. Chemical coupling has been used to functionalize magnetosomes *in vitro*,<sup>[15,16]</sup> but

often lacks selectivity and requires harsh denaturing conditions, which might abolish biological activity. In contrast, the magnetosome membrane can be manipulated *in vivo* by genetic means. Foreign functional moieties can be expressed as translational fusions to magnetosome membrane (Mam) proteins, thereby specifically targeting these cargo proteins to the magnetosome envelop. Mam proteins with non-essential and redundant functions like the highly abundant MamC have already been used as anchors for the display of fluorophores, camelid antibody fragments (nanobodies), and a variety of receptors and enzymes.<sup>[17–23]</sup> Previous studies demonstrated that magnetosome expression of cargo proteins can be increased by engineering the transcription and translation of genetic fusions. An improved magnetosome expression cassette was developed by optimizing the strong, native P<sub>mamDC</sub> promoter and the ribosome binding site (RBS) of the *mamGFDC* operon.<sup>[18]</sup> Expression of codon-optimized *egfp* (= *megfp*) as translational fusion to *mamC* resulted in 2.8-fold increased fluorescence (compared to the non-optimized system). Another reporter for magnetosome expression of gene fusions is provided by the well-characterized enzyme glucuronidase GusA from *Escherichia coli*. Using the improved expression cassette, multifunctional magnetosomes were generated by expression of mixed arrays of up to five copies of GusA and an additional terminal mEGFP (as translational reporter) as large single hybrid proteins on the magnetosome surface using MamC as membrane anchor.<sup>[23]</sup> This study also demonstrated that multimeric enzymes can be efficiently displayed on magnetosomes in high copy numbers, thereby covering up to 90% of the particle surface and triplicating the specific enzymatic activity per magnetosome.

Dr. F. Mickoleit, C. Lanzloth, Prof. D. Schüler  
Department of Microbiology  
University of Bayreuth  
Universitätsstraße 30, Bayreuth D-95447, Germany  
E-mail: Dirk.Schueler@uni-bayreuth.de

 The ORCID identification number(s) for the author(s) of this article can be found under <https://doi.org/10.1002/smll.201906922>.

© 2020 The Authors. Published by WILEY-VCH Verlag GmbH & Co. KGaA, Weinheim. This is an open access article under the terms of the Creative Commons Attribution License, which permits use, distribution and reproduction in any medium, provided the original work is properly cited.

DOI: 10.1002/smll.201906922

However, the number of MamC membrane anchors is limited to 80–250 copies per particle,<sup>[18,23,24]</sup> and simultaneous multifunctionalization by various different ligands requires the exploration of alternative magnetosome membrane proteins as potential expression anchors. For example, the integral membrane proteins MamG, MamF as well as the membrane-associated MamA were identified as highly abundant, surface-exposed Mam proteins. Because of their non-essential functions in magnetosome biosynthesis, fusions to them are not likely to interfere with magnetite biomineralization.<sup>[24–26]</sup> Their specific cellular association with magnetosomes was already demonstrated by the use of GFP fusions to MamA, MamG, and MamF.<sup>[17,24]</sup> The latter was furthermore used as single anchor protein for magnetosome display of protein A, thereby generating magnetic beads that were capable of binding the F<sub>C</sub> region of mammalian antibodies.<sup>[27,28]</sup> However, it so far remained unexplored if these Mam proteins can be utilized for simultaneous magnetosome expression of more complex, multimeric (enzyme) proteins.

In this study, we explored MamA, MamG and MamF for their use as potential magnetosome anchor proteins using mEGFP and GusA as reporters. Enzymatic activities and the amount of GusA correlated well with the estimated abundances of the respective membrane anchors (including MamC). These techniques were subsequently combined into a versatile toolkit for the highly selective magnetosome multifunctionalization. The potential of this approach was demonstrated by engineering bioconjugated magnetic nanoparticles that simultaneously display the enzyme proteins GusA and glucose oxidase (GOx), a fluorophore (mEGFP) and a nanobody (red fluorescent binding protein, RBP) on the surface. Thereby, we generated a reusable magnetic model composite, in which all displayed functionalities were fully genetically encoded and can be easily substituted by any other desired protein-based functional moieties. Thus, our synthetic biology approach can be effectively used for the generation of biohybrid nanomaterials, which have great potential for many applications in the biotechnological and biomedical field.

## 2. Results and Discussion

### 2.1. MamA, MamF, and MamG Proteins Can Be Used as Fusion Anchors for High-Level Magnetosome Display of Functional Cargo Proteins

To assess the abundances and suitability of MamA, MamF and MamG as magnetosome anchors, GusA-mEGFP reporter constructs arranged as dual tandem arrays were expressed individually as C-terminal genetic fusions to the respective Mam proteins (Figure 1). Each construct was placed behind the

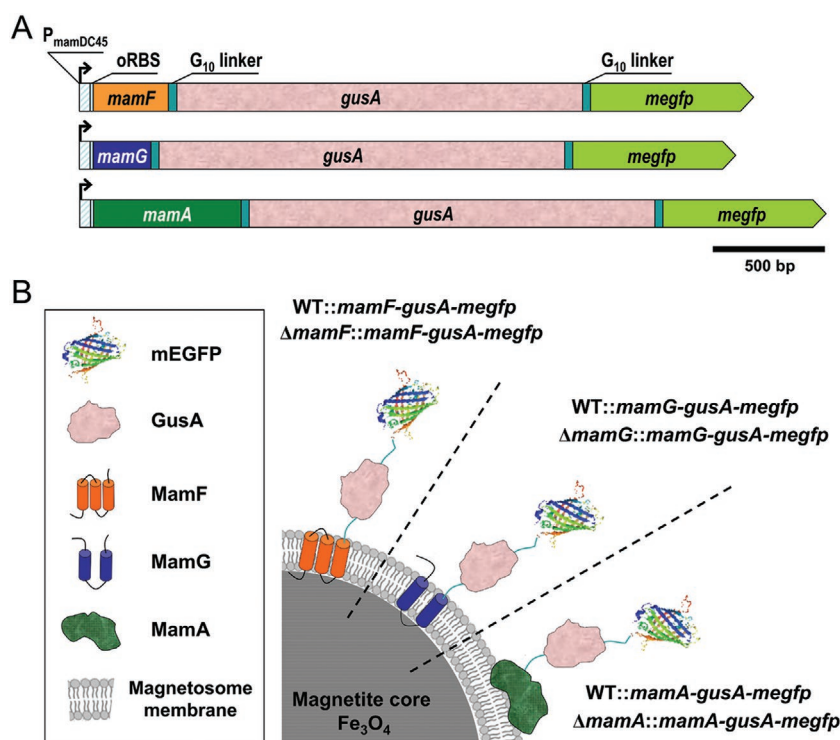


**Figure 1.** Schematic representation showing A) the genetic organization of the *gusA-megfp* expression cassettes and B) the topology of the resulting fusion proteins. The  $\beta$ -glucuronidase GusA and mEGFP were expressed as genetic fusions to MamF/G/A via G<sub>10</sub> linkers composed of ten glycine residues (size of particles and proteins not to scale). Structure models of MamF/G/A according to predictions by Nudelman and Zarivach.<sup>[33]</sup>

strong constitutive magnetosomal P<sub>mamDC45</sub> promoter with an optimized ribosome binding site (oRBS)<sup>[18]</sup> and transferred into the wildtype strain of *M. gryphiswaldense* and the respective deletion mutants ( $\Delta$ *mamA*,  $\Delta$ *mamF* or  $\Delta$ *mamG*) via conjugative Tn5 transposition.<sup>[29]</sup> The resulting chromosomal insertion strains WT::*mamA-gusA-megfp*, WT::*mamF-gusA-megfp*, WT::*mamG-gusA-megfp*,  $\Delta$ *mamA*::*mamA-gusA-megfp*,  $\Delta$ *mamF*::*mamF-gusA-megfp*, and  $\Delta$ *mamG*::*mamG-gusA-megfp* were undistinguishable from the wildtype with regard to growth, morphology and magnetosome biosynthesis. Cells of all strains displayed fluorescence signals localized at midcell, reflecting the typical position of the magnetosome chain (Figure 2A, Figure S1, Supporting Information). As expected, fluorescence intensities were lower compared to strains in which mEGFP was fused to the highly abundant MamC protein present in about 85 copies per particle (WT::*mamC-gusA-megfp* and  $\Delta$ *mamC*::*mamC-gusA-megfp*),<sup>[23]</sup> and followed the known relative abundances of the respective membrane anchors (MamC > MamA > MamF > MamG) (Figure 2B).<sup>[24,26]</sup> In the deletion strains  $\Delta$ *mamC/A/F/G* lacking the respective single wildtype alleles, signal intensities were nearly twice as high as for the corresponding complemented wildtype strains in which additional, unfused wildtype copies of the Mam anchors were still present. Assuming a roughly linear correlation between fluorescence and mEGFP copy number (as shown by Lang and Schüler<sup>[17]</sup>) 74, 62, or 56 mEGFP moieties per particles were calculated for strains  $\Delta$ *mamA*::*mamA-gusA-megfp*,  $\Delta$ *mamF*::*mamF-gusA-megfp*, and  $\Delta$ *mamG*::*mamG-gusA-megfp*, respectively (Table S1,

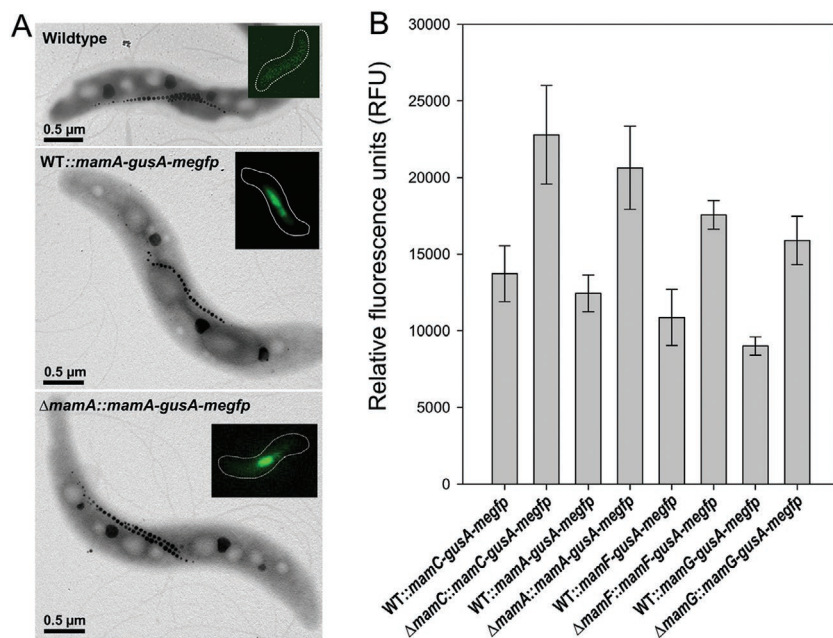


**Figure 2.** A) TEM microscopy images of representative WT::*mamA-gusA-megfp* and  $\Delta$ *mamA::mamA-gusA-megfp* cells indicated a wildtype (WT)-like phenotype with one or two magnetosome chains positioned at midcell. *megfp* expression was confirmed by fluorescence microscopy (insets), showing fluorescence signals at magnetosome chain position (for *mamF/G-gusA-megfp* expressing strains refer to Figure S1, Supporting Information). B) Cellular mEGFP fluorescence from various *gusA-megfp* fusions of *M. gryphiswaldense*. Fluorescence was normalized to cell density and reported as relative fluorescence units (RFU). Error bars represent standard deviations, calculated from at least three independent measurements. Signal intensities indicate a clear correlation with the known abundances of the utilized membrane anchors (estimated by Raschdorf et al.<sup>[24]</sup> and Grünberg et al.<sup>[26]</sup>). Values for WT::*mamC-gusA-megfp* and  $\Delta$ *mamC::mamC-gusA-megfp* taken from Mickoleit and Schüler.<sup>[23]</sup>

Supporting Information). Electrophoretic mobility of proteins solubilized from isolated magnetosomes were as predicted for the Mam-GusA-mEGFP fusion proteins (Figure 3A, Table S2, Supporting Information) indicating proper and stable expression. From band intensities in quantitative Western blots (Table S1, Supporting Information; Figure 3B) GusA amounts of 102, 74, and 69 ng GusA per  $\mu$ g Fe were calculated for strains  $\Delta$ *mamA::mamA-gusA-megfp*,  $\Delta$ *mamF::mamF-gusA-megfp*, and  $\Delta$ *mamG::mamG-gusA-megfp*, respectively, which is in good agreement with the estimated mEGFP copy numbers as calculated from fluorescence microscopy. Thus, the amount of the respective membrane anchors and cargo proteins could be estimated to be  $\approx$ 85 (MamA),  $\approx$ 66 (MamF), and  $\approx$ 60 (MamG) copies per particle (Table S1, Supporting Information).

All GusA-mEGFP magnetosome species displayed glucuronide-hydrolyzing activities (Figure 3; Figure S2 and Table S2, Supporting Information). Calculated reaction rates, which served as an indicator for the amount of catalytically active enzyme, again correlated with the GusA protein content of the particles and thus, with the relative abundances of the utilized anchor proteins. Specific activities were between 11.4 and 20.5 U  $\text{mg}^{-1}$  GusA (Table S2, Supporting Information), thus in most cases significantly higher compared to soluble GusA expressed in *M. gryphiswaldense* (12.7 U  $\text{mg}^{-1}$  GusA).<sup>[23]</sup> Specific activities per mg Fe were between 0.46 U  $\text{mg}^{-1}$  Fe (WT::*mamG-gusA-megfp*) and 1.52 U  $\text{mg}^{-1}$  Fe

( $\Delta$ *mamF::mamF-gusA-megfp*), which reflected the amount of enzyme present on the particle surface. The different GusA fusions exhibited relatively low Michaelis-Menten ( $K_M$ ) constants ( $0.12 \times 10^{-3}$  to  $0.23 \times 10^{-3}$  M) indicating high affinities for the substrate *p*-nitrophenyl- $\beta$ -D-glucuronide.<sup>[30,31]</sup> Since GusA is known to function only as a 272 kDa homotetramer,<sup>[32]</sup> the high activities indicate proper folding and assembly of GusA monomers into tetrameric structures, which apparently was not impaired by the fusions at both termini to the magnetosome anchors and mEGFP, respectively.

In contrast to MamF, MamG and MamC proteins, which are integral and tightly bound to the magnetosome membrane, MamA is only associated with the magnetosome surface and can be solubilized by mild detergents and high ionic strength.<sup>[26,33,34]</sup> However, only insignificant amounts (1.3% of the total GusA content and 1.4% glucuronide-hydrolyzing activity) of MamA-GusA-mEGFP from strain WT::*mamA-gusA-megfp* were lost during magnetosome isolation (Figure S3, Supporting Information), as shown by quantitative Western blots and enzymatic analysis of the non-magnetic fraction (i.e., the magnetosome-free flow-through). This indicated a sufficiently stable association with the magnetosome membrane of MamA as an anchor protein.

## 2.2. Generation of Multifunctional Magnetic Nanoparticles by Simultaneous Display of Various Cargo Proteins

So far, our results had demonstrated that in addition to the highly abundant MamC, the magnetosome proteins MamF, MamG and MamA are suitable anchors for stable display of individual cargo proteins, if also present in somewhat lower numbers per particle. Next, we explored whether these Mam proteins can be combined for simultaneous magnetosome display of diverse functional moieties. For that purpose, we designed a model particle that in addition to magnetization should display four additional genetically encoded functionalities: i) two different enzymatic activities (GusA and GOx), ii) the ability of versatile coupling (by expression of a nanobody), and iii) mEGFP fluorescence (Figure 4A). The latter was introduced by replacing the native *mamA* by a *mamA-megfp* fusion in the wildtype and  $\Delta$ *mamGFDC* strain of *M. gryphiswaldense* (in-frame replacement by a markerless mutagenesis approach<sup>[35]</sup>), resulting in strains  $\Delta$ *mamA::mamA-megfp* and  $\Delta$ *mamGFDC\_ΔmamA::mamA-megfp*, respectively. Next, a compact expression cassette was designed that allowed the simultaneous display of MamC fused to a RBP nanobody directed against its cognate antigen *Red Fluorescent Protein* (mCherry) as a connector, MamF fused to the glucuronidase GusA, and MamG fused to GOx (Figure 4A). GOx was chosen for magnetosome expression because it represents a more complex, i.e.

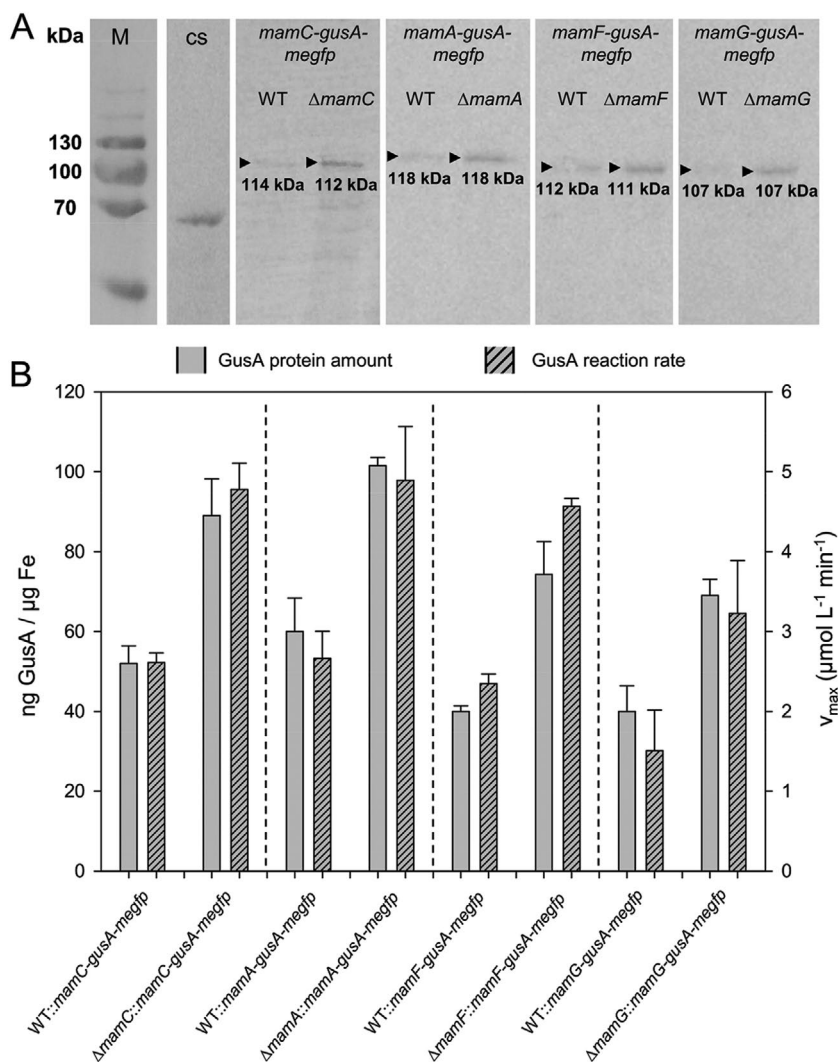


**Figure 3.** Magnetosome expression of MamC/A/F/G-GusA-mEGFP fusion proteins. The WT of *M. gryphiswaldense* and the deletion mutants  $\Delta mamC/A/F/G$  were complemented with the indicated *mam-gusA-megfp* fusions. A) Microoxically grown cells were harvested and disrupted, and the solubilized membrane fractions of isolated magnetosomes (12 or 24  $\mu\text{g}$  Fe per lane) were subjected to denaturing PAGE followed by quantitative Western blotting employing an IgG antibody directed against GusA. Electrophoretic mobility of the detected bands corresponded well to the calculated molecular masses of the fusion proteins. Degradation products potentially caused in the course of sample preparation were detected to only minor extents. Commercial, soluble GusA (cs) served as control. B) Bar chart illustrating the correlation between GusA amounts displayed on the magnetosome surface (calculated from quantitative Western blots) and GusA reaction rates ( $v_{\text{max}}$ ; calculated from kinetic measurements as the mean of Michaelis-Menten, Lineweaver-Burk, and Hanes-Woolf plots, Figure S2, Supporting Information). GusA protein amounts and  $v_{\text{max}}$  values were consistent with the known abundances of MamC/A/F/G in the magnetosome membrane. Values for WT::*mamC-gusA-megfp* and  $\Delta mamC$ ::*mamC-gusA-megfp* taken from Mickoleit and Schuler.<sup>[23]</sup>

dimeric and cofactor-dependent, enzyme with biotechnological relevance.<sup>[36]</sup> It catalyzes the oxidation of glucose yielding glucono-lactone that is subsequently hydrolyzed to gluconic acid and  $\text{H}_2\text{O}_2$ . Its glycosylation in the native host *Aspergillus niger* was shown to be dispensable for catalytic activity.<sup>[37]</sup> While chemical coupling of purified GOx to isolated magnetosomes was reported before,<sup>[38]</sup> we attempted to genetically express monomeric GOx as translational fusion to MamG in vivo. For

that purpose, the corresponding sequence from *A. niger* was back-translated and codon-optimized for *M. gryphiswaldense*. Within the  $P_{\text{mamDC45}}\text{-mamG-gox-mamF-gusA-mamC-rbp}$  expression cassette generated by Gibson Assembly (Figure S4, Supporting Information), *mamG/F/C* fusions were arranged according to their genetic organization in the *mamGFDC* operon. The  $\Delta mamA$ ::*mamA-megfp* and  $\Delta mamGFDC$  $\Delta mamA$ ::*mamA-megfp* strain of *M. gryphiswaldense* were chosen as recipients for the *mamG-gox/mamF-gusA/mamC-rbp* gene fusions. Upon chromosomal insertion, the resulting strains  $\Delta mamA$ ::*mamA-megfp* $\text{-mamG-gox-mamF-gusA-mamC-rbp}$  and  $\Delta mamGFDC$  $\Delta mamA$ ::*mamA-megfp* $\text{-mamG-gox-mamF-gusA-mamC-rbp}$  showed slower growth (doubling time of 10.4 h for the  $\Delta mamA$  background and 11.9 h for the  $\Delta mamGFDC$  $\Delta mamA$  background, compared to 6.9 and 7.5 h for untransformed parental strains, respectively). These observations might be explained by the GOx activity, which in the presence of intracellular glucose produces toxic  $\text{H}_2\text{O}_2$  that might not be fully counteracted by cellular catalase. Despite of this growth impairment, cell morphology, magnetosome arrangement and particle yields in *mamA-megfp* $\text{-mamG-gox-mamF-gusA-mamC-rbp}$  strains were undistinguishable from the wildtype ( $\Delta mamA$ ::*mamA-megfp* $\text{-mamG-gox-mamF-gusA-mamC-rbp}$ :  $26 \pm 9$  particles per cell,  $\varnothing$   $34 \pm 8$  nm;  $\Delta mamGFDC$  $\Delta mamA$ ::*mamA-megfp* $\text{-mamG-gox-mamF-gusA-mamC-rbp}$ :  $26 \pm 9$  particles per cell,  $\varnothing$   $31 \pm 9$  nm; Figure S5, Supporting Information). The four MamGFDC proteins have overlapping and partially redundant functions and act in a cooperative manner on the crystal size, with three of the four Mam proteins being sufficient to complement the  $\Delta mamGFDC$  phenotype (i.e., reduced particle sizes).<sup>[25]</sup> Thus, our data indicate the successful complementation of the  $\Delta mamGFDC$  mutation by restoration of the wildtype phenotype.

Each subunit of GOx requires one molecule of flavin adenine dinucleotide (FAD) and chelated iron to be functional,<sup>[36]</sup> which needs to be contributed by the endogenous cellular pool of the GOx-expressing host *M. gryphiswaldense*. Only small amounts of FAD were determined in the solubilized and denatured magnetosome membrane fraction of untransformed wildtype and  $\Delta mamGFDC$  strains (most probably due to unspecific binding to the membrane). In contrast, for magnetosomes of strains  $\Delta mamA$ ::*mamA-megfp* $\text{-mamG-gox-mamF-gusA-mamC-rbp}$  and  $\Delta mamGFDC$  $\Delta mamA$ ::*mamA-megfp* $\text{-mamG-gox-mamF-gusA-mamC-rbp}$  an FAD content of 19 or 32.6  $\mu\text{mol}$  per g Fe

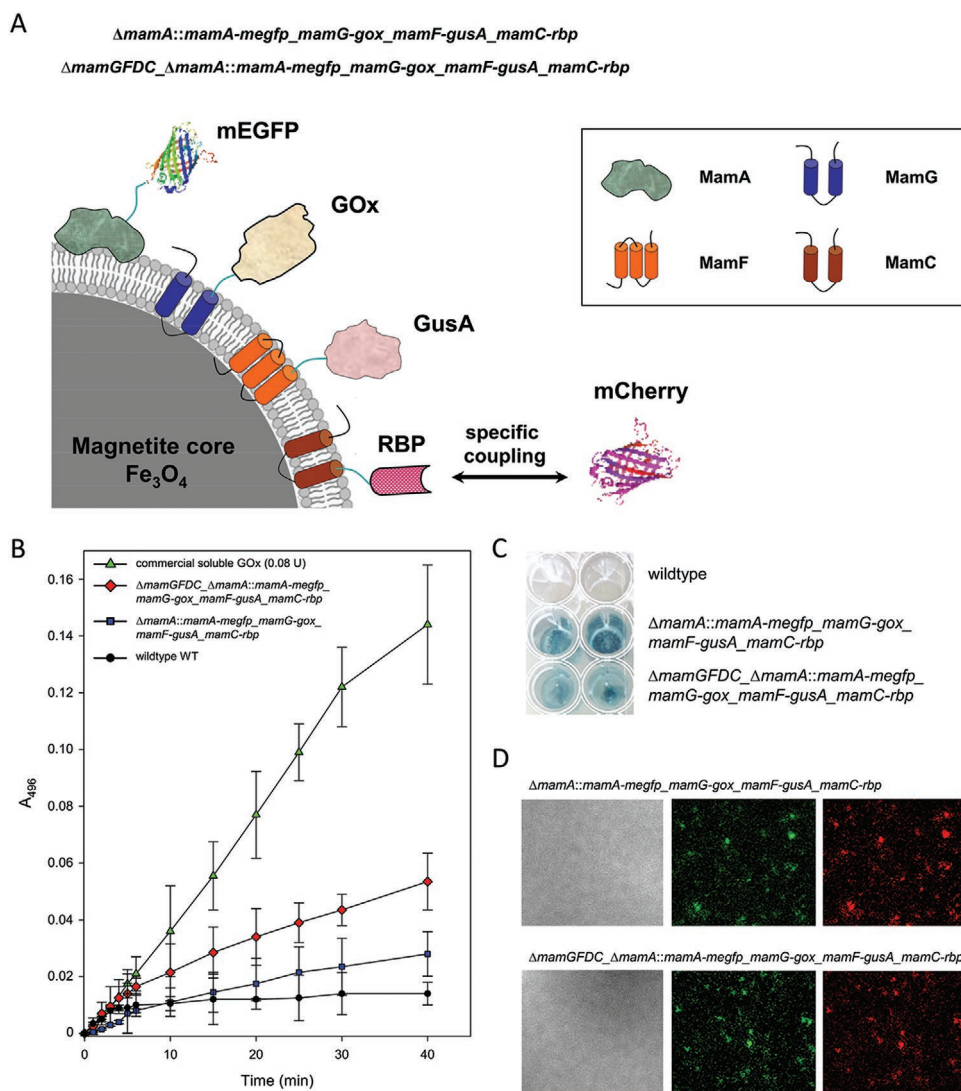


**Figure 4.** Generation of multifunctional model particles by utilization of four different Mam proteins as membrane anchors. A) Simultaneous expression of four different gene fusions (*mamA-megfp*, *mamG-gox*, *mamF-gusA*, and *mamC-rbp*) in the  $\Delta mamA$  or  $\Delta mamGFDC\_ \Delta mamA$  background allowed the surface display of mEGFP, glucose oxidase (GOx), the glucuronidase GusA, and the red fluorescent protein-binding nanobody (RBP) as versatile “connector” for coupling reactions to any RFP/mCherry-tagged structures. Size of particles and proteins not to scale. B) Isolated particles from strains  $\Delta mamA::mamA-megfp\_mamG-gox\_mamF-gusA\_mamC-rbp$  or  $\Delta mamGFDC\_ \Delta mamA::mamA-megfp\_mamG-gox\_mamF-gusA\_mamC-rbp$  were subjected to GOx activity assays employing MPMS as intermediate electron “carrier” for the reduction of INT to yield formazan (Figure S5, Supporting Information). Compared to wildtype magnetosomes, linear absorption increases were monitored, indicating glucose-oxidizing activity. C) Incubation of isolated MamA-mEGFP\_MamG-GOx\_MamF-GusA\_MamC-RBP particles with the artificial substrate X-Gluc resulted in the formation of 5,5'-dibromo-4,4'-dichloro-indigo and thus, a characteristic blue color, thereby confirming GusA activity. D) DIC (left) and fluorescence microscopy images (middle and right) of MamA-mEGFP\_MamG-GOx\_MamF-GusA\_MamC-RBP magnetosomes. Expression of mEGFP was verified by distinct fluorescence signals suggesting the formation of small magnetosome aggregates (middle). Display of functional RBP moieties was confirmed by incubating isolated particles with commercial, soluble mCherry (right). Unbound/excess protein was removed by magnetic separation and extensive washing. Fluorescence signals at identical positions as for mEGFP indicated successful binding of the fluorophore to the magnetosome surface.

was measured, roughly corresponding to 0.08 U of commercial, soluble GOx (Table S3, Supporting Information). GOx enzymatic activities are usually determined by peroxidase-based assays. However, the latter were compromised, probably by the presence of that redox-active magnetite core (data not shown).<sup>[39]</sup> Therefore, an alternative assays was adopted to quantify electron transfer reactions.<sup>[40]</sup> For magnetosomes of both strains ( $\Delta mamA::mamA-megfp\_mamG-gox\_mamF-gusA$

*mamC-rbp* and  $\Delta mamGFDC\_ \Delta mamA::mamA-megfp\_mamG-gox\_mamF-gusA\_mamC-rbp$ , each 2.5  $\mu\text{g}$  Fe) time-dependent absorption increases were monitored (Figure 4B), indicating glucose oxidizing activity. For wildtype magnetosomes (negative control) only low, insignificant background activities were detected. Since the GOx enzyme is likely to be functional as a dimer, monomers from adjacent MamG-GOx fusions might together contribute to the formation of such dimers.<sup>[41,42]</sup>

MamA-mEGFP\_MamG-GOx\_MamF-GusA\_MamC-RBP magnetosomes exhibited glucuronide-hydrolyzing activity as indicated by the conversion of the artificial substrate 5-Bromo-4-chloro-3-indolyl- $\beta$ -D-glucuronide (X-Gluc) into a blue solution (Figure 4C). Furthermore, quantitative Western blotting was used to specifically detect GusA and mEGFP in the solubilized magnetosome membrane fraction (Figure S6, Supporting Information). For both strains distinct bands of  $\approx 85$  kDa or  $\approx 50$  kDa were detected, respectively, corresponding well to the predicted molecular masses of 81.4 kDa (MamF-GusA) and 51.7 kDa (MamA-mEGFP). The amount of GusA was quantified to be 55.1 ng ( $\Delta mamA::mamA-megfp\_mamG-gox\_mamF-gusA\_mamC-rbp$ ) or 62.4 ng ( $\Delta mamGFDC\_mamA::mamA-megfp\_mamG-gox\_mamF-gusA\_mamC-rbp$ ), which is in accordance with values obtained before for MamF-GusA-mEGFP magnetosomes (Table S2, Supporting Information). In addition, MamA-mEGFP expression and mCherry binding to the magnetosome surface was confirmed by fluorescence microscopy (FM) (Figure 4D). Distinct signals were obtained at identical positions, thereby also confirming the successful display of RBP as an additional functionality. The latter might thus function as versatile “connector” for coupling reactions to any RFP-tagged structures.

### 2.3. Generation of a Magnetosome-Based Multifunctional Magnetic Hydrogel Composite

To demonstrate the potential and versatility of our approach we used mCherry-RBP antigen-nanobody interactions to generate a multifunctional model composite material displaying magnetism as well as fluorescence and two different catalytic activities. For this purpose, we coupled magnetosomes isolated from strain  $\Delta mamGFDC\_mamA::mamA-megfp\_mamG-gox\_mamF-gusA\_mamC-rbp$  to commercial, highly porous, ceramic beads (50  $\mu$ m in diameter; “Methyl Matrix–Ceramic HyperD F Hydrogel Composite”) (Figure 5A). The latter are filled with a derivatized hydrogel capable of protein binding and are commonly used in affinity chromatography.<sup>[43]</sup> When wildtype particles or magnetosomes expressing mEGFP, GOx, GusA, and RBP (Figure 5B) were mixed with the hydrogel beads in disposable polypropylene columns, a separation into two phases was observed with the magnetosomes being “repelled” and forming a distinct layer on top of the hydrogel matrix (Figure 5C). It can be assumed that the content of (functionalized) Mam proteins embedded in or attached to the magnetosome surface is not sufficient to enable interactions with the hydrogel beads. Although our multifunctionalization approach

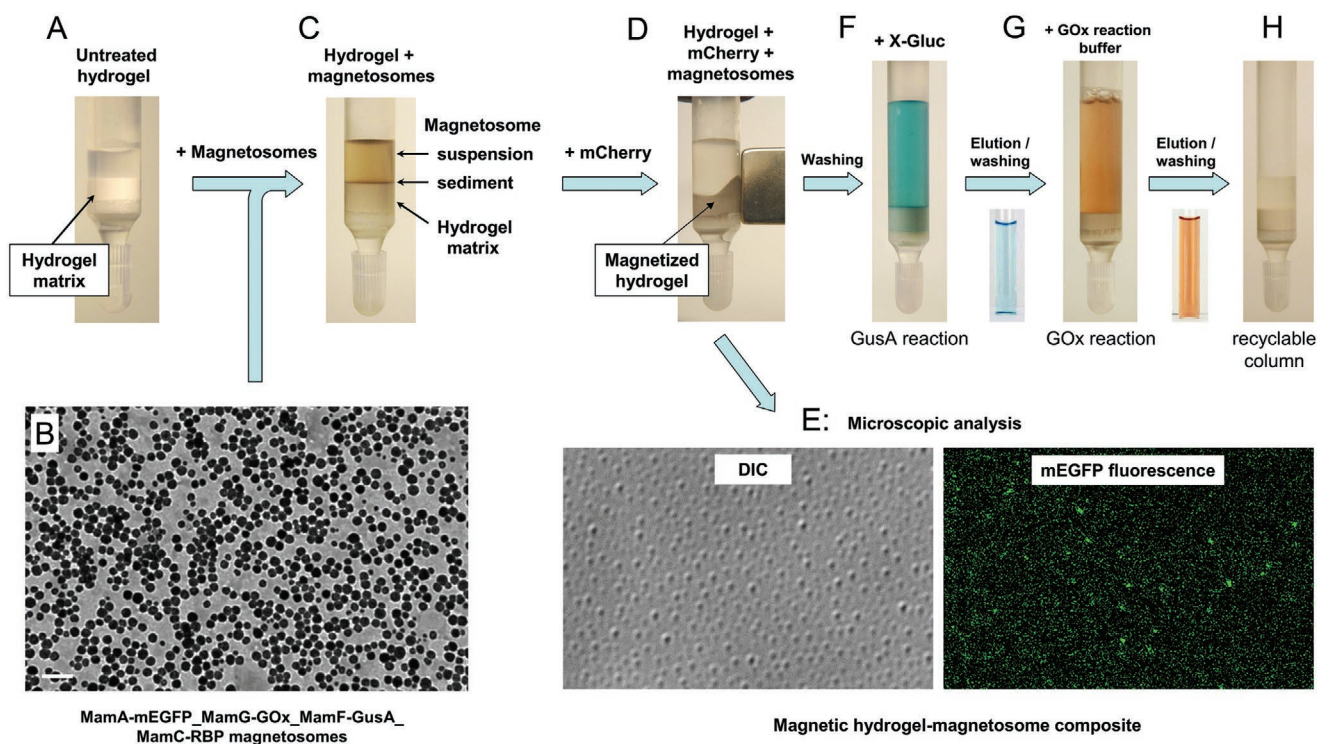


**Figure 5.** Highly porous, ceramic beads filled with a derivatized hydrogel (A; “Methyl Matrix–Ceramic HyperD F Hydrogel Composite”) were incubated with MamA-mEGFP\_MamG-GOx\_MamF-GusA\_MamC-RBP magnetosomes (B; TEM microscopy image, scale bar 100 nm). C) However, no homogenous suspension could be generated as the magnetosomes separated from the hydrogel beads forming a two-phase system and a layer on top of the matrix. D) Soluble mCherry protein was added to generate binding sites for MamA-mEGFP\_MamG-GOx\_MamF-GusA\_MamC-RBP magnetosomes. Incorporation of the latter into the matrix by mCherry-RBP antigen-nanobody interactions led to a viscous, homogenous composite material that could be attracted by the pole of a permanent magnet. E) Microscopic analysis (DIC) was used to visualize the magnetosome incubated ceramic beads, exhibiting mEGFP fluorescence. F) Furthermore, the generated magnetosome-hydrogel composite material exhibited two different catalytic activities: GusA activity was indicated by formation of bluish 5,5'-dibromo-4,4'-dichloro-indigo in the presence of X-Gluc. G) After elution and multiple washing steps, GOx reaction buffer (supplemented with  $\beta$ -D-glucose) was applied to the column. GOx activity was visualized by formation of red formazan. H) The reusability of the magnetosome-hydrogel composite was shown by repeated removal and addition of substrate. For more details, please refer to the text.

added up to 300 protein moieties in total to the surface of each magnetosome (according to the relative abundances of the different membrane anchors), still no incorporation into the matrix was observed. In order to enable specific interactions of MamA-mEGFP\_MamG-GOx\_MamF-GusA\_MamC-RBP magnetosomes with the hydrogel beads, the latter were incubated with an access of soluble mCherry protein to generate RBP binding sites. Although only about 85 MamC-RBP fusion proteins were displayed on the magnetosome surface (according to the relative abundance of MamC<sup>[23]</sup>), the mCherry-RBP antigen-nanobody interaction seemed to be strong enough to “entrap” the magnetosomes in the matrix. Thus, mixing the hydrogel beads with MamA-mEGFP\_MamG-GOx\_MamF-GusA\_MamC-RBP magnetosomes led to a homogenous, viscous suspension, indicating mCherry recognition and binding of the RBP nanobody (Figure 5D). By stable magnetosome incorporation into the hydrogel matrix, the entire composite material became magnetized, as demonstrated by attraction of the magnetosome-hydrogel composite by a permanent magnet placed closely to the slurry. Microscopic analysis by differential interference contrast (DIC) and FM confirmed the presence of the fluorescent magnetosomes within the composite (Figure 5E). Next, after multiple steps of washing, substrates for the two different enzymatic activities were added successively: First, 1 mg X-Gluc (in  $50 \times 10^{-3}$  M 4-(2-hydroxyethyl)-1-piperazineethanesulfonic acid (Hepes)/NaOH, pH 7.2) was applied to and incubated in the column. X-Gluc hydrolysis was indicated by formation of a characteristic blue color of the supernatant and the magnetosome-hydrogel suspension (Figure 5F). The 5,5'-dibromo-4,4'-dichloro-indigo containing solution was finally eluted and the column was washed several times to remove residual substrate and reaction products prior to applying 5 mL GOx reaction buffer supplemented with  $\beta$ -D-glucose. The latter was subsequently turned into a red solution (Figure 5G), illustrating the reduction of 1-phenyl-2-(4-iodo-phenyl)-3-(4-nitrophenyl)-2H-tetrazolium chloride (INT) to formazan. Repeated removal and addition of substrate led to reproducible, strong color generation over at least five cycles, indicating that the magnetosome-hydrogel composite is recyclable (Figure 5H).

### 3. Conclusion

In this study, we explored the genetic multifunctionalization of the magnetosome surface by simultaneous utilization of different magnetosome membrane proteins. The abundances of the integral MamC, MamF, and MamG, and the membrane-associated MamA proteins were estimated to be  $\approx 85$ ,  $\approx 66$ ,  $\approx 60$ , and  $\approx 85$  copy numbers per particle, and we could demonstrate that the latter can serve as stable anchors for genetic fusions with more complex, e.g. multimeric cargo proteins and tandem fusions. The genetic expression of arrays of up to five copies of GusA fused to individual MamC anchors has been shown before, thereby triplicating enzymatic activities compared to single GusA expression.<sup>[23]</sup> Implementing this strategy simultaneously to our set of different, highly abundant anchor proteins, this would greatly enhance the capacity to display foreign cargo proteins. Simultaneously functionalized, the membrane proteins MamC, MamF, MamG, and MamA would provide up

to 300 sites for covalent and highly specific attachment. Thus, the expression of arrays of up to five copies of a foreign moiety could lead to multifunctional magnetosomes with theoretically up to 1500 functional cargo proteins in total displayed on the particle surface.

Numerous in vitro strategies to generate functionalized nanoparticles are based on well-known surface chemistries and chemical coupling reactions,<sup>[15,16]</sup> however, heterogeneity and precise control over the stoichiometric number of functional moieties on the surface are still challenging issues.<sup>[44]</sup> Although chemical approaches allow for high coupling levels,<sup>[45–47]</sup> they lack specificity and are often accompanied by denaturing effects, which might lead to a loss of biological activity. In contrast, the in vivo functionalization of the magnetosome membrane by genetic engineering provides unprecedented selectivity and precise control over coupling of multiple protein cargos with variable stoichiometry.

The different proteins displayed on the surface of our engineered model particles could be easily substituted by any other desirable, non-toxic cargo moieties with biomedical or biotechnological relevance. For instance, the use of immobilized enzymes (on hydrogels or microbeads) in biocatalytic flow-reactor concepts was investigated, revealing the need for appropriate methods for the immobilization of enzymes.<sup>[48,49]</sup> Likewise, magnetosomes might serve as a versatile scaffold for the spatial organization of different catalytic activities, thereby enabling cascade reactions through the close proximity of the constituting enzyme species and balanced substrate channeling rates.<sup>[50]</sup> The feasibility to use functionalized magnetosomes as reusable, multimodal catalysts could be demonstrated in this study by incorporating MamA-mEGFP\_MamG-GOx\_MamF-GusA\_MamC-RBP magnetosomes into mCherry-equipped hydrogel-based matrices (Figure 5), which resulted in a model magnetic composite material with different catalytic activities. In addition, the introduction of molecular connectors renders magnetosomes a versatile platform that allows coupling of any cognate epitope-tagged or cellular structure. Mickleit et al., for instance, expressed streptavidin or green fluorescent binding protein (GBP) nanobodies on the particle surface.<sup>[51]</sup> The resulting magnetosomes were capable of binding biotin- or GFP-tagged particles of the tobacco mosaic virus, thereby generating a new kind of biocomposite that could serve as magnetic scaffold for adding further functionalities. Moreover, magnetosome expression/coupling of cell signaling ligands might facilitate and stabilize their oligomerization as it was shown for CD40 ligands,<sup>[52]</sup> thereby triggering signaling cascades by specific interactions with the corresponding receptors and enabling the in vitro production of therapeutic, polyclonal antibody formulations.<sup>[53]</sup>

In summary, our synthetic biology approach provides an elegant, powerful and highly selective route for the generation of engineered nanoparticles, in which *all* of the multiple functionalities (i.e., the presence of a core-shell structure, strong magnetization, fluorescence, several catalytic activities and versatile coupling groups) are fully genetically encoded. Therefore, engineered magnetosomes are highly promising as building blocks for more complex nano- and mesostructures with enhanced properties for many biotechnological and biomedical applications.

## 4. Experimental Section

**Bacterial Strains, Plasmids, and Cultivation Conditions:** Bacterial strains and plasmids that were used in this study are listed in Tables S4 and S5 (Supporting Information). *M. gryphiswaldense* strains were grown microaerobically in modified flask standard medium (FSM) at 30 °C according to Heyen and Schüler.<sup>[54]</sup> *E. coli* strains were grown as previously described.<sup>[55]</sup> For the cultivation of *E. coli* WM3064 (W. Metcalf, unpublished), D,L- $\alpha$ , $\epsilon$ -diaminopimelic acid (DAP) was added to lysogeny broth (LB) medium at a final concentration of  $1 \times 10^{-3}$  M. Strains were routinely cultured as described previously.<sup>[18,23]</sup> For the cultivation on solid medium 1.5% (w/v) agar was added, for strains carrying recombinant plasmids, media were supplemented with 25  $\mu\text{g mL}^{-1}$  kanamycin (Km) for *E. coli* or 5  $\mu\text{g mL}^{-1}$  for *M. gryphiswaldense* strains.

**Molecular and Genetic Techniques:** Oligonucleotides (see Table S6, Supporting Information) were purchased from Sigma-Aldrich (Steinheim, Germany). Plasmids were constructed by standard recombinant techniques as described in detail below.

For the construction of *M. gryphiswaldense* strains carrying *gusA-megfp* fusions (strains MSR-1 FM1 to FM6), the insertion plasmid pFM2 (which harbors a *mamC-gusA-megfp* expression cassette<sup>[23]</sup>) was subjected to double enzymatic digestion with NdeI and NcoI. *mamF*, *mamG* and *mamA* were amplified from isolated genomic DNA of *M. gryphiswaldense* MSR-1 R3/S1 using primer pairs *mamF* NdeI fwd/*mamF* NcoI rev, *mamG* NdeI fwd/*mamG* NdeI rev or *mamA* NdeI fwd/*mamA* NcoI rev, respectively. PCR products were cloned at the corresponding sites into the NdeI/NcoI restriction sites of the previously digested expression cassette of pFM2, thereby generating pFM3, pFM4, or pFM5. The latter were transferred either to the wildtype of *M. gryphiswaldense* (thereby generating strains *M. gryphiswaldense* MSR-1 FM1-3) or the corresponding isogenic deletion strains *M. gryphiswaldense*  $\Delta$ *mamF*,  $\Delta$ *mamG*, or  $\Delta$ *mamA* (which resulted in strains *M. gryphiswaldense* MSR-1 FM4-6, respectively). *mam-gusA-megfp* expression cassettes were chromosomally inserted by Tn5 transposition at random positions, allowing stable expression of the fusion proteins.

For generating magnetosomes that display several functional moieties on the surface, different Mam proteins were simultaneously utilized as membrane anchors. A chromosomal *mamA-megfp* fusion (in-frame replacement of the native *mamA*) was generated by a markerless mutagenesis approach as previously described.<sup>[35]</sup> A fragment consisting of the *mamA-megfp* sequence flanked by the upstream and downstream regions of *mamA* ( $\approx 1$  kb each) was constructed in a Gibson Assembly reaction (Table S7, Supporting Information).<sup>[56]</sup> Primers EcoRI H1-*mamA* fwd and Gibson *mamA* rev were used to amplify a sequence consisting of *mamA* and its upstream region, thereby generating a EcoRI restriction site at the 5' end and a 45 bp overhang downstream of *mamA*. *megfp* was amplified from pH1 applying primers Gibson *egfp* fwd and Gibson *egfp* rev, and primers Gibson H2 fwd and H2 BamHI rev were used to amplify the downstream region of *mamA* from genomic DNA. In all reactions, sequences with complementary, overlapping ends were generated. The fragments were simultaneously ligated and cloned at the EcoRI/BamHI restriction sites into the previously digested pFM271e\_1 using Gibson Assembly reaction, thereby generating pFM271e\_1-*mamA-megfp*. In addition, the ampicillin resistance cassette (*amp*) was amplified from pSB9 (primers Amp NheI fwd and Amp SpeI rev) and cloned into NheI/SpeI restriction sites of pFM271e\_1-*mamA-megfp*. The resulting plasmid (pFM271e\_1-*mamA-megfp\_amp*) was transferred to the wildtype and  $\Delta$ *mamGFDC* strain of *M. gryphiswaldense*.

For the construction of a *mamG-gox-mamF-gusA-mamG-rbp* expression cassette under control of the optimized  $P_{\text{mamDC45}}$  promoter, three different gene fusions were designed and ligated in a Gibson Assembly reaction,<sup>[56]</sup> Figure S4 (Supporting Information). A sequence consisting of a *gly10* linker and codon-optimized, monomeric glucose oxidase (*gly10-gox*) was synthesized by ATC:biosynthetics (Merzhausen, Germany), with NdeI or BamHI restriction sites flanking the 5' or 3' terminus, respectively. *gly10-gox* was amplified using primers GOx fwd and GOx rev and ligated into NcoI and BamHI restriction sites of pFM4 resulting in pFM1. Primers Gibson *mamG* fwd and *mamG-gox* rev were subsequently used to amplify the *mamG-gox* fragment, with an NdeI

restriction site upstream of *mamG*. *mamF-gusA* was amplified from pFM3 applying primers Gibson *mamF* fwd and Gibson *mamF-gusA* rev, and *mamC-rbp* was amplified from pAPI79<sup>[9]</sup> using primers Gibson *mamC* fwd and *rbp* rev, resulting in a fragment with a BamHI restriction site downstream of *rbp*. In all reactions, sequences with complementary, overlapping ends were generated (corresponding to the intergenic regions of the *mamGFDC* operon). The fragments were simultaneously ligated to a *mamG-gox-mamF-gusA-mamC-rbp* fusion and cloned at the NdeI/BamHI restriction sites into the previously digested pSB9 using Gibson Assembly reaction (Table S7, Supporting Information).

All constructs were sequenced by MacroGen Europe (Amsterdam, Netherlands) using the cutting edge technology. Sequence data were analyzed with Geneious 8.0.5 (Biomatters Ltd.) and ApE 2.0.47 (M. Wayne Davis, 2009).

**Spectrophotometric Measurement of Glucuronidase Activity:** The glucuronidase GusA (EC 3.2.1.31) is an acid hydrolase with a molecular weight of 68.3 kDa. It catalyzes the cleavage of 3-glucuronides, yielding 3-glucuronates and an alcohol. The enzyme is easily and sensitively assayed using commercially available glucuronide substrates.<sup>[57]</sup>

For kinetic studies on the GusA activity of isolated magnetosomes, a modified protocol from Myronovskiy et al. was used.<sup>[58]</sup> 1.0 mL (0.1–0.3  $\mu\text{g Fe}$ ) of purified particles in dilution buffer ( $5 \times 10^{-3}$  M DTT, 0.1% Triton X-100, pH 7.0) were centrifuged and incubated at 37 °C for 15 min. Finally, 5–100  $\mu\text{L}$  0.2 M *p*-nitrophenyl- $\beta$ -D-glucuronide were added to the magnetosome pellet to start the time-dependent reaction (carried out at 37 °C). The production of *p*-nitrophenol was monitored by measuring the optical density at 415 nm ( $\text{OD}_{415}$ ). As reference, 1.0 mL dilution buffer without magnetosomes was used. Units were micromoles ( $\mu\text{mol}$ ) of product formed per minute at 37 °C. Reported values were averaged from at least three independent cultures.

For qualitative determination/assessment of the GusA activity, the commercial substrate X-Gluc (5-bromo-4-chloro-3-indolyl- $\beta$ -D-glucuronic acid, cyclohexylammonium salt) was used. 100  $\mu\text{L}$  cell suspension of isolated magnetosomes were supplemented with 100  $\mu\text{g}$  X-Gluc (10  $\mu\text{L}$  of a 10 mg  $\text{mL}^{-1}$  stock solution). X-Gluc was hydrolyzed by magnetosome-bound GusA yielding glucuronic acid and 5-bromo-4-chloro-indoxyl. The latter was subsequently oxidized to 5,5'-dibromo-4,4'-dichloro-indigo, resulting in a characteristic blue color.

**GOx Activity Assay:** For measuring glucose oxidizing activity of GOx displaying magnetosomes, an assay which had previously been used to quantify enzyme-based electron transfer reactions was modified.<sup>[49]</sup> 250  $\mu\text{L}$   $\beta$ -D-glucose solution (0.5 M) was added to 1 mL oxygen-saturated reaction buffer (123.75  $\times 10^{-6}$  M INT, 22.25  $\times 10^{-6}$  M 1-methoxyphenazine 5-methosulfate (MPMS), 0.625 (w/v) Triton X-100 in  $50 \times 10^{-3}$  M  $\text{KH}_2\text{PO}_4/\text{NaOH}$  pH 7.2) and incubated at 35 °C for 5 min. The reaction was started by adding 50  $\mu\text{L}$  magnetosome suspension (with a defined Fe content), and the time-dependent absorption increase  $A_{496\text{nm}}$  was monitored for at least 35 min (Evolution 201 UV-Vis spectrophotometer; Thermo Scientific Instruments, Madison, Wisconsin, USA). A solution of commercial glucose oxidase (0.08 U  $\text{mL}^{-1}$ ) served as positive control. In the assay, electrons released in the course of glucose oxidation were transferred to the intermediate electron "carrier" MPMS. The latter finally reduced INT yielding formazan, whose formation could be monitored at 496 nm (Figure S7, Supporting Information).

**Determination of FAD:** To investigate whether FAD became inserted and remained bound to the magnetosome-associated GOx monomers in vivo, the magnetosome membrane fraction was solubilized and the protein compounds denatured and precipitated, thereby releasing enzyme-bound cofactors. FAD was determined in supernatants neutralized with  $2.4 \times 10^{-3}$  M  $\text{K}_2\text{HPO}_4$  from its absorption at 450 nm in the oxidized and reduced state, employing the molar differential extinction coefficient  $\epsilon_{450}$  of FAD.<sup>[59,60]</sup>

**Determination of Iron Concentrations:** Iron contents of cells and isolated magnetosomes were determined by flame atomic absorption spectroscopy. For that purpose, appropriate (e.g., 1:10–1:100) dilutions of the corresponding fractions were prepared. Magnetosomes or cells (suspensions of equal optical density) were pelleted, resuspended in 0.5 mL 69% nitric acid and digested at 98 °C for 3 h. The measurements

were conducted with a Perkin-Elmer Atomic Absorption Spectrometer 1100 B (Überlingen, Germany) using the following conditions: wavelength 248.3 nm, gap width 0.2 nm, lamp current 20 mA.

**Analytical Methods:** Optical density (OD) and magnetic response ( $C_{mag}$ ) of late exponentially phase cells were measured photometrically at 565 nm as previously reported.<sup>[61]</sup> Magnetosome expression of mEGFP or mCherry-binding to RBP was assayed by fluorescence microscopy (Olympus IX81 microscope equipped with a Hamamatsu Orca AG camera) as described before.<sup>[17]</sup> Briefly, to verify the expression of RBP nanobodies on the magnetosome surface, purified MamA-mEGFP\_MamG-GOx\_MamF-GusA\_MamC-RBP magnetosomes were incubated with commercial, soluble mCherry. After removal of unbound fluorophore by magnetic separation and multiple washing steps, mCherry-loaded particles were analyzed by fluorescence microscopy. Image rescaling and cropping were performed with Corel Photopaint 12.0 and GIMP (GNU Image Manipulation Program) 2.8.10 software.

For TEM of whole cells and isolated magnetosomes, specimens were directly deposited onto carbon-coated copper grids (Science Services, Munich, Germany). Magnetosomes were stained with 1% uranyl acetate. Transmission electron microscopy was performed on a CEM 902A (Zeiss, Oberkochen, Germany) with an acceleration voltage of 80 kV. Images were taken with a Gata Erlangshen ES500W CCD camera. Sizes of crystals were measured with ImageJ software.

**Biochemical Methods:** Isolation of bacterial magnetosomes from *M. gryphiswaldense* was performed as previously described.<sup>[17,54]</sup> Denaturing polyacrylamide gels were prepared according to the method of Laemmli,<sup>[62]</sup> modified after Fling and Gregerson.<sup>[63]</sup> Magnetosome membrane protein fractions solubilized from isolated particles (0.5–10 µg Fe) were separated by electrophoresis and subsequently transferred onto polyvinylidene difluoride (PVDF) membranes (Roth, Germany). Immunochemical detection of Mam-GusA fusion proteins was performed as previously described,<sup>[23]</sup> using a rabbit anti-GusA IgG primary antibody (Antibodies-Online, Aachen, Germany) at a 1:7500 ratio. IgG antibodies specific for GFP (Santa Cruz Biotechnology, Heidelberg, Germany) were applied to detect MamA-mEGFP in the magnetosome membrane fraction (ratio 1:3000).

**Incorporation of Magnetosomes into Hydrogel-based Matrices:** Magnetosome-hydrogel bead composites were generated by incubating 1.5 mL “Methyl Matrix: Ceramic HyperD F Hydrogel Composite” (provided as aqueous ethanol suspension, 50 µm mean particle size; Sigma-Aldrich, Steinheim, Germany) with soluble mCherry protein (TP790040; OriGene, Herford, Germany). The composite was subsequently filled into disposable polypropylene columns (Thermo Fisher Scientific, Dreieich, Germany) prior to adding/resuspending the indicated magnetosome suspensions.

## Supporting Information

Supporting Information is available from the Wiley Online Library or from the author.

## Acknowledgements

The authors are grateful to Sarah Borg for providing expression plasmids and Frank Müller for providing the pFM271e\_1 counterselection vector. The authors also thank Matthias Schlotter (Department of Microbiology, University of Bayreuth) for expert technical assistance. Aileen Jakobs, Sebastian A. Pirner, Vanessa Köberlin, and Felix Gaile are acknowledged for contributing some of the data produced as part of their Bachelor's theses at the Department of Microbiology (University of Bayreuth). This project was funded in part from the Deutsche Forschungsgemeinschaft (Grant No. Schu 1080/9-2) and the European Research Council (ERC) under the European Union's Horizon 2020 research and innovation program (Grant No. 692637 to D.S.).

## Conflict of Interest

The authors declare no conflict of interest.

## Keywords

magnetic composites, magnetosomes, *Magnetospirillum gryphiswaldense*, nanoparticles, synthetic biology

Received: November 29, 2019

Revised: February 21, 2020

Published online: March 18, 2020

- [1] C. Jogler, D. Schüler, *Annu. Rev. Microbiol.* **2009**, *63*, 501.
- [2] F. Nudelman, N. A. Sommerdijk, *Angew. Chem., Int. Ed.* **2012**, *51*, 6582.
- [3] D. Faivre, T. U. Godec, *Angew. Chem., Int. Ed.* **2015**, *54*, 4728.
- [4] R. Uebe, D. Schüler, *Nat. Rev. Microbiol.* **2016**, *14*, 621.
- [5] D. Faivre, D. Schüler, *Chem. Rev.* **2008**, *108*, 4875.
- [6] D. Faivre, L. H. Böttger, B. F. Matzanke, D. Schüler, *Angew. Chem., Int. Ed.* **2007**, *46*, 8495.
- [7] D. A. Bazylinski, R. B. Frankel, *Nat. Rev. Microbiol.* **2004**, *2*, 217.
- [8] E. Alphandéry, A. T. Ngo, C. Lefèvre, I. Lisiecki, L. F. Wu, M. P. Pileni, *J. Phys. Chem. C* **2008**, *112*, 12304.
- [9] Y. Pan, N. Petersen, M. Winklhofer, A. F. Davila, Q. Liu, T. Frederichs, M. Hanzlik, R. Zhu, *Earth Planet. Sci. Lett.* **2005**, *237*, 311.
- [10] X. Zhu, S. S. Kalirai, A. P. Hitchcock, D. A. Bazylinski, *J. Electron Spectrosc. Relat. Phenom.* **2015**, *199*, 19.
- [11] C. Carvalho, P. Sainctavit, M. A. Arrio, N. Menguy, Y. Wang, G. Ona-Nguema, S. Brice-Profeta, *Am. Mineral.* **2008**, *93*, 880.
- [12] R. Weissleder, A. Moore, U. Mahmood, R. Borhade, H. Benveniste, E. A. Chiocca, J. P. Basilion, *Nat. Med.* **2000**, *6*, 351.
- [13] J.-H. Lee, Y.-M. Huh, Y. Jun, J. Seo, J. Jang, H.-T. Song, S. Kim, E.-J. Cho, H.-G. Yoon, J.-S. Suh, J. Cheon, *Nat. Med.* **2007**, *13*, 95.
- [14] R. Hergt, S. Dutz, M. Röder, *J. Phys.: Condens. Matter* **2008**, *20*, 385214.
- [15] B. Ceyhan, P. Alhorn, C. Lang, D. Schüler, C. M. Niemeyer, *Small* **2006**, *2*, 1251.
- [16] R. Wacker, B. Ceyhan, P. Alhorn, D. Schüler, C. Lang, C. M. Niemeyer, *Biochem. Biophys. Res. Commun.* **2007**, *357*, 391.
- [17] C. Lang, D. Schüler, *Appl. Environ. Microbiol.* **2008**, *74*, 4944.
- [18] S. Borg, J. Hofmann, A. Pollithy, C. Lang, D. Schüler, *Appl. Environ. Microbiol.* **2014**, *80*, 2609.
- [19] A. Pollithy, T. Romer, C. Lang, F. D. Müller, J. Helma, H. Leonhardt, U. Rothbauer, D. Schüler, *Appl. Environ. Microbiol.* **2011**, *77*, 6165.
- [20] S. Borg, F. Popp, J. Hofmann, H. Leonhardt, U. Rothbauer, D. Schüler, *mBio* **2015**, *6*, pii: e02117.
- [21] S. Ohuchi, D. Schüler, *Appl. Environ. Microbiol.* **2009**, *75*, 7734.
- [22] N. Ginot, R. Pardoux, G. Adryanczyk, D. Garcia, C. Brutesco, D. Pignol, *PLoS One* **2011**, *6*, e21442.
- [23] F. Mickoleit, D. Schüler, *Adv. Biosyst.* **2018**, *2*, 1700109.
- [24] O. Raschdorf, F. Bonn, N. Zeytuni, R. Zarivach, D. Becher, D. Schüler, *J. Proteomics* **2018**, *172*, 89.
- [25] A. Scheffel, A. Gärdes, K. Grünberg, G. Wanner, D. Schüler, *J. Bacteriol.* **2008**, *190*, 377.
- [26] K. Grünberg, E. C. Müller, A. Otto, R. Reszka, D. Linder, M. Kube, R. Reinhardt, D. Schüler, *Appl. Environ. Microbiol.* **2004**, *70*, 1040.
- [27] J. Xu, J. Hu, L. Liu, L. Li, X. Wang, H. Zhang, W. Jiang, J. Tian, Y. Li, J. Li, *Front. Microbiol.* **2014**, *5*, 136.
- [28] J. Xu, L. Liu, J. He, S. Ma, S. Li, Z. Wang, T. Xu, W. Jiang, Y. Wen, Y. Li, J. Tian, F. Li, *J. Nanobiotechnol.* **2019**, *17*, 37.

- [29] D. Schultheiss, D. Schüler, *Arch. Microbiol.* **2003**, 179, 89.
- [30] *Enzyme Handbook*, Vol. 4 (Eds: D. Schomburg, M. Salzmann), Springer, Berlin **1991**, pp. 105–113.
- [31] B. D. Wallace, A. B. Roberts, R. M. Pollet, J. D. Ingle, K. A. Biernat, S. J. Pellock, M. K. Venkatesh, L. Guthrie, S. K. O'Neal, S. J. Robinson, M. Dollinger, E. Figueroa, S. R. McShane, R. D. Cohen, J. Jin, S. V. Frye, W. C. Zamboni, C. Pepe-Ranney, S. Mani, L. Kelly, M. R. Redinbo, *Chem. Biol.* **2015**, 22, 1238.
- [32] B. D. Wallace, H. Wang, K. T. Lane, J. E. Scott, J. Orans, J. S. Koo, M. Venkatesh, C. Jobin, L. A. Yeh, S. Mani, M. R. Redinbo, *Science* **2010**, 330, 831.
- [33] H. Nudelman, R. Zarivach, *Front. Microbiol.* **2014**, 5, 9.
- [34] N. Zeytuni, E. Ozyamak, K. Ben-Harush, G. Davidov, M. Levin, Y. Gat, T. Moyal, *Proc. Natl. Acad. Sci. USA* **2011**, 108, E480.
- [35] O. Raschdorf, J. M. Plitzko, D. Schüler, F. D. Müller, *Appl. Environ. Microbiol.* **2014**, 80, 4323.
- [36] S. B. Bankar, M. V. Bule, R. S. Singhal, L. Ananthanarayan, *Biotechnol. Adv.* **2009**, 27, 489.
- [37] H. M. Kalisz, J. Hendle, R. D. Schmid, *Appl. Microbiol. Biotechnol.* **1997**, 47, 502.
- [38] T. Matsunaga, S. Kamiya, *Appl. Microbiol. Biotechnol.* **1987**, 26, 328.
- [39] J. M. Byrne, N. Klugle, C. Pearce, K. M. Rosso, E. Appel, A. Kappler, *Science* **2015**, 347, 1473.
- [40] A. M. Pelzmann, F. Mickoleit, O. Meyer, *JBIC J. Biol. Inorg. Chem.* **2014**, 19, 1399.
- [41] K. R. Frederick, J. Tung, R. S. Emerick, F. R. Masiarz, S. H. Chamberlain, A. M. I. T. Vasavada, S. Rosenberg, S. Chakraborty, L. M. Schopfer, V. Massey, *J. Biol. Chem.* **1990**, 265, 3793.
- [42] S. Ferri, K. Kojima, K. Sode, *J. Diabetes Sci. Technol.* **2011**, 5, 1068.
- [43] J. Pezzini, V. B. Brochier, M. P. Barrouillet, M. Cerruti, G. Clofent-Sanchez, A. Schapman, A. Topol, R. Robert, C. Cabanne, P. Cerruti, X. Santarelli, *J. Chromatogr. B* **2009**, 877, 2428.
- [44] J. Gao, H. Gu, B. Xu, *Acc. Chem. Res.* **2009**, 42, 1097.
- [45] W. S. Seo, J. H. Lee, X. Sun, Y. Suzuki, D. Mann, Z. Liu, M. Terashima, P. C. Yang, M. V. McConnell, D. G. Nishimura, H. Dai, *Nat. Mater.* **2006**, 5, 971.
- [46] X. Michalet, F. F. Pinaud, L. A. Bentolila, J. M. Tsay, S. Doose, J. J. Li, G. Sundaresan, A. M. Wu, S. S. Gambhir, S. Weiss, *Science* **2005**, 307, 538.
- [47] J. Shin, R. M. Anisur, M. K. Ko, G. H. Im, J. H. Lee, I. S. Lee, *Angew. Chem., Int. Ed.* **2009**, 48, 321.
- [48] T. Peschke, P. Bitterwolf, S. Gallus, Y. Hu, C. Oelschlaeger, N. Willenbacher, K. S. Rabe, C. M. Niemeyer, *Angew. Chem.* **2018**, 130, 17274.
- [49] T. Peschke, P. Bitterwolf, S. Hansen, J. Gasmir, K. S. Rabe, C. M. Niemeyer, *Catalysts* **2019**, 9, 164.
- [50] X.-Y. Qiu, S.-S. Xie, L. Min, X.-M. Wu, L.-Y. Zhu, L. Zhu, *Microb. Cell Fact.* **2018**, 17, 120.
- [51] F. Mickoleit, K. Altintoprak, N. L. Wenz, R. Richter, C. Wege, D. Schüler, *ACS Appl. Mater. Interfaces* **2018**, 10, 37898.
- [52] F. Mickoleit, V. Jérôme, R. Freitag, D. Schüler, *Adv. Biosyst.* **2020**, 1900231, <https://doi.org/10.1002/adbi.201900231>.
- [53] M. Radosevich, T. Burnouf, *Vox Sang.* **2010**, 98, 12.
- [54] U. Heyen, D. Schüler, *Appl. Microbiol. Biotechnol.* **2003**, 61, 536.
- [55] J. Sambrook, D. Russell in *Molecular Cloning: A Laboratory Manual*, 3rd ed. Cold Spring Harbor Laboratory Press, New York, NY **2001** pp. 1–44.
- [56] D. G. Gibson, L. Young, R. Y. Chuang, J. C. Venter, C. A. Hutchison III, H. O. Smith, *Nat. Methods* **2009**, 6, 343.
- [57] R. A. Jefferson, S. M. Burgess, D. Hirsh, *Proc. Natl. Acad. Sci. USA* **1986**, 83, 8447.
- [58] M. Myronovskiy, E. Welle, V. Fedorenko, A. Luzhetskyy, *Appl. Environ. Microbiol.* **2011**, 77, 5370.
- [59] L. G. Whitby, *Biochem. J.* **1953**, 54, 437.
- [60] W. R. Waud, F. O. Brady, R. D. Wiley, K. V. Rajagopalan, *Arch. Biochem. Biophys.* **1975**, 169, 695.
- [61] D. Schüler, R. Uhl, E. Bäuerlein, *FEMS Microbiol. Lett.* **1995**, 132, 139.
- [62] U. K. Laemmli, *Nature* **1970**, 227, 680.
- [63] S. P. Fling, D. S. Gregerson, *Anal. Biochem.* **1986**, 155, 83.